https://doi.org/10.1016/j.snb.2023.133379

A new fluorescent biosensor based on inner filter effect and competitive coordination with the europium ion of non-luminescent Eu-MOF nanosheets for the determination of alkaline phosphatase activity in human serum

Shuisheng Hu [1,a,b,c], Jingyan Liu [1,a], Yong Wang [c], Zhiguang Liang [c], Bin Hu [a], Jiahe Xie [a,d], Wing-Leung Wong [c,*], Kwok-Yin Wong [c], Bin Qiu [b,*] Weijie Peng [a,*]

[a] Key Laboratory of Prevention and Treatment of Cardiovascular and Cerebrovascular Diseases, Ministry of Education, Key Laboratory of Biomaterials and Biofabrication in Tissue Engineering of Jiangxi Province, Key Laboratory of Biomedical Sensors of Ganzhou, School of Medical and Information Engineering, Scientific Research Center, Gannan Medical University, Ganzhou, Jiangxi, 341000, P. R. China.

[b] Ministry of Education Key Laboratory of Analytical Science of Food Safety and Biology, Fujian Provincial Key Laboratory of Analysis and Detection for Food Safety, Fuzhou University, Fuzhou, Fujian, 350108, P. R. China.

[c] State Key Laboratory of Chemical Biology and Drug Discovery, Department of Applied Biology and Chemical Technology, The Hong Kong Polytechnic University, Hung Hom, Kowloon, Hong Kong SAR, P. R. China.

[d] Department of Cardiology, First Affiliated Hospital of Gannan Medical University, Gannan Medical University, University Town, Ganzhou Development District, Ganzhou, 341000, P.R. China.

[1] These authors contributed equally to this work.

* Corresponding author:

E-mail: summer328cn@163.com (B. Qiu); wing.leung.wong@polyu.edu.hk (W.L. Wong); weijiepeng@126.com (W.J. Peng).

Tel: 86-591-22866135

Address: Department of Chemistry, Fuzhou University, Fuzhou, Fujian, 350108, China

Abstract

The abnormal level of alkaline phosphatase (ALP) in human blood stream indicates health problem. A novel fluorescent sensing system based on competitive coordination with europium ions (Eu^{3+}) integrated in a non-luminescent lanthanide-metal organic framework nanosheets (NO_2-Eu-MOF NS) was developed for ALP analysis in human serum. The fluorescence signal is turned-on by the antenna ligand (1,4-phenylenediphosphonic acid (PEPP)) that competitively coordinates with Eu^{3+} ions from the nanosheet to produce emissive species ($Eu_x(PEPP)_y(NO_2BDC)_z$) *in-situ*. 4-Nitrophenyl phosphate (PNPP) is a substrate of ALP and specifically hydrolyzed into 4-nitrophenol. PNPP exhibits a strong absorption in the UV-Vis region (250-400 nm), which covers the excitation wavelength (280 nm) of $Eu_x(PEPP)_y(NO_2BDC)_z$. Therefore, the existing of PNPP causes $Eu_x(PEPP)_y(NO_2BDC)_z$ non-emissive and, after hydrolysis with ALP, $Eu_x(PEPP)_y(NO_2BDC)_z$ can be excited and give a detectable fluorescence signal. Based on the fluorescence change, quantitative analysis of ALP activity is thus achievable. This biosensing system was demonstrated in the determination of ALP activity with good linear relationship in the range of 5-1000 U L^{-1}. The limit of detection was 1.1 U L^{-1} (S/N=3). The result reveals that the biosensor exhibits excellent sensing performance and anti-interference ability. It could be potentially utilized for clinical routine analysis of ALP activity in human serum.

Keywords: Nitro-modified lanthanide metal organic framework; competitive coordination; two-dimensional nanosheet; alkaline phosphatase; inner filter effect.

1. Introduction

Fluorescence detection techniques are important and commonly used analytical methods for chemical, biological and medical studies. The rational design and synthesis of fluorescent sensing probes with different materials can develop specific sensors for reporting sensor-target interactions. In human body, alkaline phosphatase (ALP) is a vital enzyme and is primarily found in liver, bones, intestine, and kidneys [1]. The abnormal level of ALP in blood may reflect health problems such as liver or bone diseases [2]. Despite a number of analytical methods such as colorimetric [3], surface enhance Raman spectroscopy (SERS) [4], electrochemical [5], electrochemiluminescence (ECL) method [6], and isotope labeling method [7] has been reported to determine the activity of ALP, fluorescence is regard as one of the most sensitive and attractive strategies because of its high sensitivity and selectivity for rapid detection [8, 9]. More importantly, fluorescent sensor is feasible for point-of-care (POC) applications. With respect to different sources of fluorescent signal, methods reported for ALP activity analysis can be generally divided into the following categories: noble metal materials [10], quantum dots [11], organic dyes [12], and metal nanoclusters [13]. However, these analytical methods encounter certain disadvantages such as cumbersome synthesis process [14], poor solubility [15], complicated operation, time-consuming process, cytotoxicity and poor specificity. These factors limit the fabrication of ALP-specific biosensors for practical and clinical applications. It is therefore necessary to establish a novel analytical strategy with the merit property of high selectivity and sensitivity, easy operation, and low-cost for rapid detection and monitoring of ALP level in human serum.

Recently, lanthanide ion (Ln^{3+})-based fluorescent sensors have attracted great attention owing to their unique optical properties, such as larger stokes shift, narrow emission band, and long fluorescence lifetime. However, the challenge is difficult to excite Ln^{3+} in solvent or solution due to its low absorption cross sections and the non-radiative deactivation through the O−H

vibrations of the coordinated water molecules. Therefore, the addition of chelating agents or encapsulation of lanthanide ions is required to enhance emission lifetimes and quantum yields [16]. The emission intensity of Ln^{3+} can also be significantly enhanced upon chelating with suitable ligands such as antenna that can transfer energy to the emissive state of Ln^{3+} ions. Thus, ligands with antenna property are commonly used to absorb energy and transfer it to Ln^{3+} ions for excitation [17].

Fluorescent sensors based on lanthanides have been widely utilized for the detection of anions [18], metal ions [19], biology molecules [20], and pH value [21] in human serum. In addition, co-doped lanthanide complexes and materials have been reported [22]. They are mainly used in laser devices because of their excellent fluorescence characteristics in solid state; however, their application as fluorescent sensors in solution system are rarely investigated. Recently, a lanthanide-based metal organic framework (Ln-MOF) has been reported and demonstrated some merit fluorescence properties including sharp emission peaks, large stocks shift, long fluorescence lifetime and high quantum yield in solution systems [22], which could be developed as the attractive biosensors. In addition, MOFs have many attractive properties such as high surface area, easy obtained, easy modify and good thermal stability and these merits make MOF be useful materials in many fields including catalysis, separation, gas storage drug delivery and sensing [23]. Therefore, the incorporation of Ln^{3+} ions into a MOF system may develop sensitive and robust sensing system for different analytical purposes. For example, Qian and co-workers fabricated a selective PO_4^{3-} sensor based on Tb-MOF ($TbNTA{\cdot}H_2O$) [24]. Zhou and co-workers synthesized two Ln-MOFs, $[Eu(BPDC)(BDC)_2(H_2O)_2]_n$ and $[Tb(BPDC)(BDC)_2(H_2O)_2]_n]$, which exhibited good selectivity towards F^- ions in solution [25].

The primary interaction between sensing targets and Ln-MOF-based sensors is through host–guest electron transfer. Most Ln-MOFs are applied directly to fabricate fluorescent sensors

because of the strong fluorescence properties of the materials. There are only few works about the non-luminescent Ln-MOF reported to date. In the present study, we reported a novel Ln-MOF sensor, which is non-luminescent in the long wavelength region (> 550 nm). The non-luminescent Ln-MOF system is designed with the nitro-coordinated europium (non-luminescent in 550-800 nm), which is integrated into a two-dimensional metal organic frameworks nanosheet (NO_2-Eu-MOF NS) as a "turn-on" signaling agent. The luminescence of the Eu^{3+} complex in solution can be restored selectively via the interaction with the target analyte, 1,4-phenylenediphosphonic acid (PEPP), which is an antenna ligand. The as-synthesized NO_2-Eu-MOF NS was fully characterized by SEM, TEM, AFM, XPS, XRD, and BET. In addition, the NO_2-Eu-MOF NS was demonstrated as a selectively and sensitively biosensor for the determination of ALP in human serum based on the different UV-Vis absorption properties between 4-nirtrophenyl phosphate and 4-nitrophenol.

2. Experimental Section

2.1. Synthesis of NO_2-Eu-MOF NS

NO_2-Eu-MOF NS was synthesized by solvothermal method. $Eu(NO_3)_3 \cdot 6H_2O$ (178 mg, 40 mM) was dissolved in 0.95 mL H_2O. Nitroterephthalic acid (NO_2BDC, 105.5 mg, 50 mM) and 2-fluorobenzoic acid (48.7 mg, 35 mM) were dissolved in 9 mL DMF with sonication. The $Eu(NO_3)_3$ solution and concentrated nitrate acid (50 μL) were added into the NO_2BDC solution dropwise with stirring. After 10 min, the mixture was transferred into a Teflon lined hydrothermal autoclave reactor. Then, the reaction was heated to 180 °C for 12 h. After cooling down to room temperature, the solid products obtained were washed consecutively two times with DMF, followed by DI water and other two times with absolute ethanol. The resulting materials were dried at 100 °C under vacuum condition overnight. A white powder was obtained for further characterization.

2.2. Fluorescence assays for the determination of ALP activity

The PEPP (10 mM) was added into NO_2-Eu-MOF NS (50 μL, 100 μg mL^{-1}) solution for 10 min. and the solution of ALP with various activity was added to PNPP solution (25 mM) at 35 °C for 20 min. Then, the ALP − PNPP mixed solution was added into NO_2-Eu-MOF NS/PEPP solution and then was incubated for 30 min in room temperature. After that, Tris-HCl (50 mM, pH 9.0) was added to the mixture to make the final volume of the reaction to 200 μL. The fluorescence emissions spectra from 550 to 800 nm were measured with the excitation wavelength at 280 nm. The relationships between the fluorescence intensity (FL intensity) and the activity of ALP were plotted as a calibration plot.

3. Result and discussion

3.1. Characterization of NO_2-Eu-MOF NS

The morphology and structure of NO_2-Eu-MOF NS were investigated with SEM, TEM and AFM. From **Fig. 1 a** to **c**, the SEM images shows that the synthesized NO_2-Eu-MOF NS has uniform appearance and is a two-dimensional nanosheet. Moreover, from the TEM images shown in **Fig. 1 d** to **f**, the NO_2-Eu-MOF NS is a strip-like nanosheet. The EDS images (**Fig. 1 g** to **k**) also confirm that the composition of NO_2-Eu-MOF NS includes C, O, N, and Eu elements. To investigate the thickness of NO_2-Eu-MOF NS, the strip-like nanosheet was broken down into small pieces with sonication. The AFM images obtained (**Fig. S1**) indicate that the thickness of NO_2-Eu-MOF NS is 4.6 nm approximately.

The position here for Fig. 1

The XPS survey spectrum of NO_2-Eu-MOF NS was shown in **Fig. S2**. The results indicate that NO_2-Eu-MOF NS is composited by Eu, C, N and O elements. The high-resolution XPS spectra of NO_2-Eu-MOF NS were shown in **Fig. 2**. The binding energy of Eu 3d in the nanosheet was

1125 eV - 1175 eV. The result is consistent with that of $Eu(NO_3)_3$. From **Fig. 2a**, the binding energies for Eu^{3+} were found at 1135.77 eV (Eu^{3+} $3d_{5/2}$) and 1165.7 eV (Eu^{3+} $3d_{3/2}$). In addition, the binding energies at 1128.68 eV (Eu^{2+} $3d_{5/2}$) and 1157.87 eV (Eu^{2+} $3d_{3/2}$) observed may suggest that Eu^{2+} ions may also present in NO_2-Eu-MOF NS [26]. The C 1s spectra shown in **Fig. 2b** reveal that the binding energy in 284.1 eV is corresponding to the C-C bonds in benzene ring; the 285.85 eV suggests the C-O bond in carboxylate group of NO_2BDC; 188.6 eV suggests the C-N bond of NO_2BDC in NO_2-Eu-MOF NS [27]. The O 1s spectra were shown in **Fig. 2c**. It is assigned to be Eu-O bond in 530.42 eV and the binding energy at 533.29 eV is corresponding to the C-O bond in carboxylate group, and the peak at 533.29 eV is attributed to the N-O bond of the NO_2 group of NO_2BDC [28]. **Fig. 2d** shows the N 1s spectra of NO_2-Eu-MOF NS. The binding energy at 398.86 eV, 400.22 eV, and 401.51 eV were assigned to be C-N, Ar-N-O, and NO_2 group bond in NO_2-Eu-MOF NS, respectively [29]. All these results confirm evidently the formation of NO_2-Eu-MOF NS.

The position here for Fig. 2

The XRD spectra of NO_2-Eu-MOF NS (**Fig. S3 a**) also show the characteristic peaks at 2θ of 8.14°, 16.40° and 24.67°, which are corresponding to the (2 0 0), (4 0 0) and (6 0 0) peaks, respectively. These peaks are similar to that of NH_2-Eu-MOF reported by Liu and co-workers [30]. A signature peak of NO_2-Eu-MOF NS observed with the strongest intensity at 8.14° may suggest that NO_2-Eu-MOF NS is well-crystallized [31]. In addition, NO_2-Eu-MOF NS was characterized with FT-IR (**Fig S2 b**). The asymmetric stretching of the carboxylate group (V_{as}C-O) in NO_2BDC is located at 1574-1669 cm^{-1} and the symmetric stretching (V_sC-O) appears at 1385 cm^{-1} and 1429 cm^{-1} [32]. The porous property of NO_2-Eu-MOF NS was shown in **Fig S2 c** and **d**. The BET surface area estimated is 13.9 m^2g^{-1} and the pore size is 6.4 nm. The low BET surface area may be

attribute to the bulk materials that were formed from the stacking of several layers of nanosheets [33].

3.2. Study the working principle of NO_2-Eu-MOF NS as a fluorescent biosensor

In the design of NO_2-Eu-MOF NS for biosensing applications, the non-emissive Eu^{3+} ions integrated in NO_2-Eu-MOF NS is the key fluorescence "turn-on" switch. Due to the quenching effect attributed from the withdrawing nitro groups and non-radiative vibrations of NO_2BDC [30], the NO_2-Eu-MOF NS in solution in the long wavelength region 550-800 nm is therefore non-fluorescence. However, the intrinsic fluorescence property of these Eu^{3+} ions integrated in the nanosheet can be restored by the suitable antenna effect [34]. We propose a working principle of applying NO_2-Eu-MOF NS as a distinctive fluorescent biosensor targeting ALP enzyme that hydrolyzes PNPP into 4-NP in solution [35]. In this sensing system (**Scheme 1**), the fluorescence of Eu^{3+} ions coordinated with NO_2BDC in the nanosheet is quenched in solution; however, in the presence of 1,4-phenylenediphosphonic acid (PEPP), the NO_2BDC coordinated with Eu^{3+} is substituted by PEPP to form $Eu_x(PEPP)_y(NO_2BDC)_z$ as a new complex. It is because the phosphate group of PEPP has much higher affinity with Eu^{3+} ions than the carboxylate group of NO_2BDC. $Eu_x(PEPP)_y(NO_2BDC)_z$ is an emissive complex with strong emission in the range of 550-800 nm upon excited at 280 nm in solution. PNPP exhibits a strong UV-Vis absorption in 250-300 nm, which is able to quench the fluorescence of $Eu_x(PEPP)_y(NO_2BDC)_z$ via inner filter effect (IFE). In the absence of ALP, PNPP quenches the fluorescence of $Eu_x(PEPP)_y(NO_2BDC)_z$. In the presence of ALP, PNPP is hydrolyzed to 4-NP. The intensity of fluorescence signal due to $Eu_x(PEPP)_y(NO_2BDC)_z$ is thus recovered and the change of fluorescence intensity is proportional to the concentration of PNPP in solution. As a result, based on the relationship between fluorescence intensity and the activity of ALP, a specific fluorescent biosensor is able to

fabricate to determine ALP activity in human serum.

The position here for Scheme 1

3.3. Study the feasibility and mechanism of the proposed sensor

NO_2-Eu-MOF NS (M) in solution exhibited no emission in the range of 550-800 nm upon excited at 280 nm (**Fig. 3 a**), due to the quenching effect from the nitro group and non-radiative vibrations of NO_2BDC. NO_2BDC shows a small peak located at 470 nm (λ_{ex} = 280 nm). When NO_2BDC coordinates with Eu^{3+} ion to form NO_2-Eu-MOF NS, the fluorescence peak located at 470 nm is blue shifted to 432 nm due to ligand-to-metal charge transfer in NO_2-Eu-MOF NS [36]. Upon the addition of PEPP to NO_2-Eu-MOF NS, PEPP competes with NO_2BDC to coordinate with Eu^{3+} ions from M and then to produce emissive $Eu_x(PEPP)_y(NO_2BDC)_z$ and free NO_2BDC. The fluorescence at 432 nm was red shifted to 460 nm and three new fluorescence peaks at 596 nm, 619 nm and 704 nm were observed due to the Eu^{3+} in $Eu_x(PEPP)_y(NO_2BDC)_z$, which were induced by energy transition of $^5D_0 \rightarrow {}^7F_1$, $^5D_0 \rightarrow {}^7F_2$ and $^5D_0 \rightarrow {}^7F_4$ [37]. These fluorescence peaks are also observed in EuPEPP, indicating that $Eu_x(PEPP)_y(NO_2BDC)_z$ may have similar a structure to EuPEPP. The XRD spectra of M, $Eu_x(PEPP)_y(NO_2BDC)_z$, EuPEPP and EuPEPP-simulation were given in **Fig. 3 b** for comparison. The XRD spectrum of EuPEPP synthesized in the present study is consistent with the reported results (EuPEPP-simulation) [38], indicating the complex is obtained successfully. The result obtained also supports a competitive binding mechanism between PEPP and NO_2BDC in NO_2-Eu-MOF NS. Furthermore, our observation was in accord with the previous reported work that revealed competitive binding could be occurred by different solubility product constant between Eu^{3+} binding with phosphate groups and Eu^{3+} binding with carboxylate groups [39].

Moreover, most XRD peaks of $Eu_x(PEPP)_y(NO_2BDC)_z$ are observed in that of EuPEPP and M, which may support that the structure of $Eu_x(PEPP)_y(NO_2BDC)_z$ is similar to that of EuPEPP. The amorphous morphology of $Eu_x(PEPP)_y(NO_2BDC)_z$ was shown in **Fig. 3 c**. The EDX results of $Eu_x(PEPP)_y(NO_2BDC)_z$ indicate that the elements C, Eu, O, P and N in $Eu_x(PEPP)_y(NO_2BDC)_z$ were evenly distributed. In addition, the SEM images of EuPEPP were given in **Fig. S4** for the comparison and it was found that the amorphous morphology of EuPEPP was similar to that of $Eu_x(PEPP)_y(NO_2BDC)_z$. The structure translation from M to $Eu_x(PEPP)_y(NO_2BDC)_z$ was applied to fabricate fluorescence sensors for ALP activity determination. As shown in **Fig. 3 d**, M with PEPP (10 mM) has the highest fluorescence emission, which is originated from $Eu_x(PEPP)_y(NO_2BDC)_z$. The fluorescence was quenched when PNPP was added into M with PEPP (10 mM) system, while the ALP did not affect the fluorescence of M with PEPP (10 mM) system. As previous work reported that PNPP was hydrolyzed by ALP into 4-nitrophnol (4-NP). in the present of ALP, the enhanced fluorescence compared with the absence of sample and the recovered of fluorescent intensity is proportional to the amount of ALP added. To investigate the fluorescence quenching and recovering mechanism, the UV-Vis spectrum of PNPP was obtained as shown in **Fig. 3e**. The UV absorption of PNPP is located at 250-400 nm. The peak absorption is at about 300 nm, which overlaps with the excitation wavelength of $Eu_x(PEPP)_y(NO_2BDC)_z$ complex. The quenching of the observed fluorescence is due to attenuation of excitation beam, which is known as primary IFE [39]. The UV-Vis absorption of 4-NP is about 300-470 nm and the peak is located at about 400 nm, which has no effect on the fluorescence of $Eu_x(PEPP)_y(NO_2BDC)_z$ complex. Therefore, an enhancement of fluorescence intensity is observed. The enhanced fluorescent intensity is proportional the amount of ALP added.

The position here for Fig. 3

3.4. Optimization of sensing conditions for the biosensor

The parameters including PEPP concentration, PNPP concentration, the reaction time of PEPP with NO_2-Eu-MOF NS and the time of ALP hydrolysis PNPP to 4-NP, which may affect the sensing performance of the proposed biosensors, were optimized. As shown in **Fig. 4 a**, the concentration of PEPP was varied to react with NO_2-Eu-MOF NS (100 μg mL^{-1}) to obtain the highest fluorescence intensity. The signal intensity was enhanced with the increase of PEPP concentration and reached a plateau at 10 mM, which was thus chosen as the optimized concentration. The reaction time of PEPP with NO_2-Eu-MOF NS was also optimized. As shown in **Fig. 4 b**, when the time was at 10 min, which was arrived the plateau of FL intensity compared with 15 and 20 min. Therefore, 10 min was chosen as the optimum reaction time of PEPP with NO_2-Eu-MOF NS. PNPP was applied as a ALP substrate that could quench the fluorescence of $Eu_x(PEPP)_y(NO_2BDC)_z$, its concentration was corresponding to the activity ALP, so it was essentially to be optimized. As shown in **Fig. 4 c**, with increasing the concentration of PNPP, the FL intensity was reduced and then arrived a plateau at 25 mM. The reaction time for ALP hydrolysis PNPP was optimized, As shown in **Fig. 4 d**, the fluorescence intensity was changed along with the reaction time and reached a plateau after 20 min. Then, 20 min was chosen as the optimum for the hydrolysis of PNPP by ALP. As shown in **Fig. S5**, the FL intensity reached the maximum when ALP was added under the condition at pH 9.0, so the optimal pH value of buffer was chosen as 9.0, which was able to offer the highest ALP activity. The FL intensity of system without ALP was found very stable in different pH conditions, indicating that the fluorescence property of $Eu_x(PEPP)_y(NO_2BDC)_z$ was not influenced by the change of pH conditions [40].

The position here for Fig. 4

3.5 The determination of ALP activity with the biosensor

Fig. 5 a shows the fluorescence intensity with a variety of activity of ALP under the optimized conditions. The signal intensity gradually increased with the increase of ALP activity in the range of 5-1000 U L^{-1}. **Fig. 5 b** shows the linear relationship between the ΔF and the activity of ALP. The D-value of the fluorescence intensity (ΔF) is calculated by the equation: $\Delta F=F-F_0$. Where F_0 is the fluorescence intensity of the $Eu_x(PEPP)_y(NO_2BDC)_z$ solution after being quenched by PNPP; F is the fluorescence intensity of the $Eu_x(PEPP)_y(NO_2BDC)_z$ solution after ALP hydrolyzed PNPP into 4-NP. A correlation coefficient of 0.998 was obtained. The linear equation established from the quantitative assay is $\Delta F = 0.52C_{(ALP)} + 1.92$ and the limit of detection (LOD) was found to be 1.1 U L^{-1} (S/N=3). The recently reported sensing systems for the determination of ALP activity were summarized in **Table 1** for comparison. It was found that the LOD of our fabricated sensor based on NO_2-Eu-MOF NS is lower than most of reported sensors. Furthermore, the new sensor developed in this work shows better reproducibility.

The position here for Fig. 5

3.6 Selectivity and interferential tests for the biosensor

Selectivity is one of the key metrics to evaluate the performance of sensors and needs to be investigated. The substances selected for the evaluation of selectivity and anti-interference ability of the proposed sensor include inorganic ions such as copper nitrate (Cu^{2+}), magnesium chloride (Mg^{2+}), sodium sulfide (S^{2-}), zinc nitrate (Zn^{2+}), iron nitrate (Fe^{3+}), and tetrasodium pyrophosphate (PPi), amino acids in human blood such as glutathione (GSH), threonine (Thr), lysine (Lys) and tryptophan (Trp), and the enzymes similar to ALP such as acid phosphatase (ACP) and inorganic pyrophosphatase (PPase). The uric acid (UA), glucose (Glu), human serum albumin (HSA), and adenosine

triphosphate (ATP). The concentration of these substrates was applied with respect to their normal concentrations found in human blood. The evaluation result was shown in **Fig. 6**. From **Fig. 6 a**, the fluorescence intensity of all these substrates showed no significant interference to the biosensor compared to the blank (the biosensor solution alone), whereas the addition of ALP induced an intensive fluorescence signal. In addition, from **Fig. 6 b**, all these substrates showed no significant influence to ALP to induce fluorescence signal. These results illustrate that these interferences examined almost have no significant effects on the sensing performance of the biosensor. The results may suggest that the proposed biosensor has excellent selectivity and anti-interferential ability for ALP activity analysis.

The position here for Fig. 6

The position here for Table 1

3.7. Determination of ALP activity in human serum

To validate the feasibility of using NO_2-Eu-MOF NS for routine and practical analysis, the determination of ALP activity in real human serum was performed. Three human serum samples were obtained from First Affiliated Hospital of Gannan Medical University. The activities of ALP of these samples determined by our biosensor were 88.20 U L^{-1}, 76.10 U L^{-1} and 59.30 U L^{-1}, respectively. The results are very comparable with the activity given by the hospital (**Table 2**: 90, 78 and 60 U L^{-1}). In addition, the recoveries were examined using the method of standard addition. Three serum samples were spiked with standard solution of ALP (10.0 U L^{-1}, 50.0 U L^{-1}, and 100.0 U L^{-1}, respectively). The spiked concentration is chosen based on the normal activity of ALP in human serum, which is in the range of 40-160 U L^{-1} [41]. The recovery observed with NO_2-Eu-MOF NS fabricated biosensor was in the range of 95.0-103.6% (**Table 2**) and the relative

standard deviation (RSD) was ranged from 4.5% to 5.5%. The analytical results indicate that the present biosensing protocol based on NO_2-Eu-MOF NS is feasible and reliable for the determination of ALP activity from human serum samples.

The position here for Table 2

4. Conclusion

In conclusion, nitro-modified two-dimensional metal organic framework nanosheets, NO_2-Eu-MOF NS, were synthesized to be a new non-luminescent Ln-MOF. The non-emissive Eu^{3+} ions integrated in the NO_2-Eu-MOF NS is the key fluorescence "turn-on-off-on" switch to fabricate biosensor for ALP activity analysis in real human serum samples with high sensitivity, selectivity and reliability. The mechanistic study showed that, firstly, the enhanced fluorescent signal was attributed to the antenna ligand (PEPP) competing with the quencher (NO_2BDC) in the NO_2-Eu-MOF NS to coordinate with the integrated Eu^{3+} ions and followed to produce the emissive $Eu_x(PEPP)_y(NO_2BDC)_z$ *in-situ*. Secondly, the fluorescence of $Eu_x(PEPP)_y(NO_2BDC)_z$ was quenched by 4-nitrophenyl phosphate (PNPP) via inner filter effect. Thirdly, the fluorescence was "turn-on" in the present of ALP because the enzyme hydrolyzed PNPP into 4-NP. Thus, the quench effect from PNPP was interrupted. Furthermore, the fluorescence response of system was demonstrated to be highly selective to ALP against a panel of substrates commonly existing in the human serum. This new analytical protocol developed based on a non-luminescent Ln-MOF, NO_2-Eu-MOF NS, may show great potential in practical and clinical applications for the determination of ALP activity.

CRediT authorship contribution statement

Shuisheng Hu and **Jinyan Liu**: Writing-original draft, Formal analysis, Data curation,

Investigation. **Yong Wang** and **Zhiguang Liang**: Formal analysis. **Bin Hu**: Data curation. **Jiahe Xie**: Resources. **Wing-Lueng Wong**: Writing-review & editing, Visualization, Funding acquisition. **Kwok-Yin Wong**: Visualization, Supervision. **Weijie Peng**: Resources, Validation. **Bin Qiu**: Methodology, Writing-review & editing, Supervision.

Declaration of competing interest

The authors declare that they have no known competing financial interests or personal relationships that could have appeared to influence the work reported in this paper.

Acknowledgements

The authors gratefully acknowledge the financial support of the Health and Medical Research Fund (HMRF), Hong Kong SAR (Project No. 19200231); PolyU Startup Fund (No. P0035712, P0043754); PolyU SZRI Fund (No. P0039278). The Jiangxi Provincial Natural Science Foundation (No. 20224BAB213008), The Open Project Program of Key Laboratory for Analytical Science of Food Safety and Biology, Ministry of Education (No. FS2201). The startup fund (No. QD202134) support from the Gannan medical university.

Reference

[1] X. Huang, X. Bian, L. Chen, L. Guo, B. Qiu, Z. Lin, Highly sensitive homogeneous electrochemiluminescence biosensor for alkaline phosphatase detection based on click chemistry-triggered branched hybridization chain reaction, Anal Chem. 93(2021) 10351-10357.

[2] H. Orimo, The mechanism of mineralization and the role of alkaline phosphatase in health and disease, J Nippon Med Sch. 77(2010) 4-12.

[3] J. An, Y. Hu, G. Liu, M. Chen, R. Chen, Y. Lyu, M. Yuan, M. Luo, Y. Liu, A fluorometric and colorimetric dual-signal nanoplatform for ultrasensitive visual monitoring of the activity of alkaline phosphatase, J Mater Chem B. 9(2021) 2998-3004.

[4] X. Dai, L. Lu, X. Zhang, Z.-L. Song, W. Song, Q. Chao, Q. Li, W. Wang, J. Chen, G.-C. Fan, MnO_2 shell-isolated SERS nanoprobe for the quantitative detection of ALP activity in trace serum: Relying on the enzyme-triggered etching of MnO_2 shell to regulate the signal, Sens Actuators, B. 334(2021) 129605.

[5] L. Sappia, B. Felice, M.A. Sanchez, M. Martí, R. Madrid, M.I. Pividori, Electrochemical sensor for alkaline phosphatase as biomarker for clinical and in vitro applications, Sens Actuators, B. 281(2019) 221-228.

[6] X.-Y. Yang, Y.-Y. Bai, Y.-Y. Huangfu, W.-J. Guo, Y.-J. Yang, D.-W. Pang, Z.-L. Zhang, Ultrasensitive electrochemiluminescence biosensor based on closed bipolar electrode for alkaline phosphatase detection in single liver cancer cell, Anal Chem. 93(2020) 1757-1763.

[7] X. Liu, Z.-H. Cheng, S.-Q. Zhang, N. Wu, T. Yang, M.-L. Chen, J.-H. Wang, Amplification strategy of silver nanoclusters with a satellite-nanostructure for substrate-free assay of alkaline phosphatase by ICP-MS, Anal Chem. 92(2020) 3769-3774.

[8] D. Zhao, J. Li, C. Peng, S. Zhu, J. Sun, X. Yang, Fluorescence immunoassay based on the alkaline phosphatase triggered in situ fluorogenic reaction of o-phenylenediamine and ascorbic acid, Anal Chem. 91(2019) 2978-2984.

[9] L. Hou, Y. Qin, J. Li, S. Qin, Y. Huang, T. Lin, L. Guo, F. Ye, S. Zhao, A ratiometric multicolor fluorescence biosensor for visual detection of alkaline phosphatase activity via a smartphone, Biosens Bioelectron. 143(2019) 111605.

[10] H. Liu, M. Li, Y. Xia, X. Ren, A turn-on fluorescent sensor for selective and sensitive detection of alkaline phosphatase activity with gold nanoclusters based on inner filter effect, ACS Appl Mater Interfaces. 9(2017) 120-126.

[11] F. Niu, Y.-L. Ying, X. Hua, Y. Niu, Y. Xu, Y.-T. Long, Electrochemically generated green-fluorescent N-doped carbon quantum dots for facile monitoring alkaline phosphatase activity based on the Fe3+-mediating ON-OFF-ON-OFF fluorescence principle, Carbon. 127(2018) 340-348.

[12] J. Ou-Yang, C.-Y. Li, Y.-F. Li, B. Yang, S.-J. Li, An infinite coordination polymer nanoparticles-based near-infrared fluorescent probe with high photostability for endogenous alkaline phosphatase in vivo, Sens Actuators, B. 255(2018) 3355-3363.

[13] Y. Hu, Y. He, Y. Han, Y. Ge, G. Song, J. Zhou, Determination of the activity of alkaline

phosphatase based on aggregation-induced quenching of the fluorescence of copper nanoclusters, Microchim Acta. 186(2019) 1-8.
[14] X. Tong, J. Xiang, X. Lu, P.-L. Karsenti, Y. Zhao, Electrically enhancing and modulating the photoluminescence of upconversion nanoparticles using liquid crystals, J Mater Chem C. 6(2018) 7683-7688.
[15] L. Xu, X. He, Y. Huang, P. Ma, Y. Jiang, X. Liu, S. Tao, Y. Sun, D. Song, X. Wang, A novel near-infrared fluorescent probe for detecting intracellular alkaline phosphatase and imaging of living cells, J Mater Chem B. 7(2019) 1284-1291.
[16] P.K.-L. Fu, C. Turro, Energy transfer from nucleic acids to Tb (III): selective emission enhancement by single DNA mismatches, J Am Chem Soc. 121(1999) 1-7.
[17] H. Tan, B. Liu, Y. Chen, Luminescence nucleotide/Eu3+ coordination polymer based on the inclusion of tetracycline, J Phys Chem C. 116(2012) 2292-2296.
[18] Y.-W. Wang, S.-B. Liu, Y.-L. Yang, P.-Z. Wang, A.-J. Zhang, Y. Peng, A terbium (III)-complex-based on–off fluorescent chemosensor for phosphate anions in aqueous solution and its application in molecular logic gates, ACS Appl Mater Interfaces. 7(2015) 4415-4422.
[19] H. Tan, B. Liu, Y. Chen, Lanthanide coordination polymer nanoparticles for sensing of mercury (II) by photoinduced electron transfer, ACS nano. 6(2012) 10505-10511.
[20] K. Staszak, K. Wieszczycka, V. Marturano, B. Tylkowski, Lanthanides complexes–Chiral sensing of biomolecules, Coord Chem Rev. 397(2019) 76-90.
[21] Y. Huang, B. Liu, Q. Shen, X. Zhu, Y. Hao, Z. Chang, F. Xu, P. Qu, M. Xu, Lanthanide coordination polymer probe for time-gated luminescence sensing of pH in undiluted human serum, Talanta. 164(2017) 427-431.
[22] J.N. Hao, D. Niu, J. Gu, S. Lin, Y. Li, J. Shi, Structure engineering of a lanthanide-based metal–organic framework for the regulation of dynamic ranges and sensitivities for pheochromocytoma diagnosis, Adv Mater. 32(2020) 2000791.
[23] W. Shi, W. Li, W. Nguyen, W. Chen, J. Wang, M. Chen, Advances of metal organic frameworks in analytical applications, Mater Today Adv. 15(2022) 100273.
[24] H. Xu, Y. Xiao, X. Rao, Z. Dou, W. Li, Y. Cui, Z. Wang, G. Qian, A metal–organic framework for selectively sensing of PO43− anion in aqueous solution, J Alloys Compd. 509(2011) 2552-2554.
[25] J.-M. Zhou, W. Shi, N. Xu, P. Cheng, Highly selective luminescent sensing of fluoride and organic small-molecule pollutants based on novel lanthanide metal–organic frameworks, Inorg Chem. 52(2013) 8082-8090.
[26] T. Alammar, I.Z. Hlova, S. Gupta, A. Biswas, T. Ma, L. Zhou, V. Balema, V.K. Pecharsky, A.-V. Mudring, Mechanochemical synthesis, luminescent and magnetic properties of lanthanide benzene-1, 4-dicarboxylate coordination polymers (Ln 0.5 Gd 0.5) 2 (1, 4-BDC) 3 (H 2 O) 4; Ln= Sm, Eu, Tb, New J Chem. 44(2020) 1054-1062.
[27] A.E. Vilian, B. Dinesh, R. Muruganantham, S.R. Choe, S.-M. Kang, Y.S. Huh, Y.-K. Han, A screen printed carbon electrode modified with an amino-functionalized metal organic

framework of type MIL-101 (Cr) and with palladium nanoparticles for voltammetric sensing of nitrite, Microchim Acta. 184(2017) 4793-4801.
[28] J. Ren, X. Du, W. Zhang, M. Xu, From wheat bran derived carbonaceous materials to a highly stretchable and durable strain sensor, RSC Adv. 7(2017) 22619-22626.
[29] E. Mazzotta, S. Rella, A. Turco, C. Malitesta, XPS in development of chemical sensors, RSC Adv. 5(2015) 83164-83186.
[30] P. Yi, H. Huang, Y. Peng, D. Liu, C. Zhong, A series of europium-based metal organic frameworks with tuned intrinsic luminescence properties and detection capacities, RSC Adv. 6(2016) 111934-111941.
[31] H. Chen, G. Zheng, M. Li, Y. Wang, Y. Song, C. Han, J. Dai, Z. Fu, Photo-and thermo-activated electron transfer system based on a luminescent europium organic framework with spectral response from UV to visible range, Chem Commun. 50(2014) 13544-13546.
[32] H.C. Woo, D.K. Yoo, S.H. Jhung, Highly Improved Performance of Cotton Air Filters in Particulate Matter Removal by the Incorporation of Metal–Organic Frameworks with Functional Groups Capable of Large Charge Separation, ACS Appl Mater Interfaces. 12(2020) 28885-28893.
[33] T. Rodenas, I. Luz, G. Prieto, B. Seoane, H. Miro, A. Corma, F. Kapteijn, F.X.L. i Xamena, J. Gascon, Metal–organic framework nanosheets in polymer composite materials for gas separation, Nat Mater. 14(2015) 48-55.
[34] X.-L. Qu, D. Gui, X.-L. Zheng, R. Li, H.-L. Han, X. Li, P.-Z. Li, A Cd (II)-based metal–organic framework as a luminance sensor to nitrobenzene and Tb (III) ion, Dalton Trans. 45(2016) 6983-6989.
[35] Z. Kahveci, M.J. Martinez-Tome, R. Mallavia, C.R. Mateo, Fluorescent biosensor for phosphate determination based on immobilized polyfluorene–liposomal nanoparticles coupled with alkaline phosphatase, ACS Appl Mater Interfaces. 9(2017) 136-144.
[36] X. Yin, Y. Song, Y. Wang, L. Zhang, Q. Li, Synthesis, structure and luminescence properties of metal-organic frameworks based on benzo-bis (imidazole), Sci China: Chem. 57(2014) 135-140.
[37] J. Zhang, L. Dai, A.M. Webster, W.T.K. Chan, L.E. Mackenzie, R. Pal, S.L. Cobb, G.L. Law, Unusual magnetic field responsive circularly polarized luminescence probes with highly emissive chiral europium (III) complexes, Angew Chem, Int Ed. 60(2021) 1004-1010.
[38] Z. Amghouz, S. García-Granda, J.R. Garcia, A. Clearfield, R. Valiente, Organic–inorganic hybrids assembled from lanthanide and 1, 4-phenylenebis (phosphonate), Cryst Growth Des. 11(2011) 5289-5297.
[39] X. Tang, H. Yu, B. Bui, L. Wang, C. Xing, S. Wang, M. Chen, Z. Hu, W. Chen, Nitrogen-doped fluorescence carbon dots as multi-mechanism detection for iodide and curcumin in biological and food samples, Bioact Mater. 6(2021) 1541-1554.
[40] Y. Xu, H. Yu, L. Chudal, N.K. Pandey, E.H. Amador, B. Bui, L. Wang, X. Ma, S. Deng, X. Zhu, Striking luminescence phenomena of carbon dots and their applications as a double

ratiometric fluorescence probes for H_2S detection, Mater Today Phys. 17(2021) 100328.
[41] K. Phoonsawat, K. Khachornsakkul, N. Ratnarathorn, C.S. Henry, W. Dungchai, Distance-Based Paper Device for a Naked-Eye Albumin-to-Alkaline Phosphatase Ratio Assay, ACS Sens. 6(2021) 3047-3055.
[42] D.-E. Wang, X. Gao, G. Li, T. Xue, H. Yang, H. Xu, Facile colorimetric assay of alkaline phosphatase activity using polydiacetylene liposomes with calcium ions and pyrophosphate, Sens Actuators, B. 289(2019) 85-92.
[43] Z. Gao, K. Deng, X.-D. Wang, M. Miró, D. Tang, High-resolution colorimetric assay for rapid visual readout of phosphatase activity based on gold/silver core/shell nanorod, ACS Appl Mater Interfaces. 6(2014) 18243-18250.
[44] Q. Hu, B. Zhou, F. Li, J. Kong, X. Zhang, Turn-on colorimetric platform for dual activity detection of acid and alkaline phosphatase in human whole blood, Chem - Asian J. 11(2016) 3040-3045.
[45] Q. Hu, M. He, Y. Mei, W. Feng, S. Jing, J. Kong, X. Zhang, Sensitive and selective colorimetric assay of alkaline phosphatase activity with Cu (II)-phenanthroline complex, Talanta. 163(2017) 146-152.
[46] M. Cai, C. Ding, F. Wang, M. Ye, C. Zhang, Y. Xian, A ratiometric fluorescent assay for the detection and bioimaging of alkaline phosphatase based on near infrared Ag_2S quantum dots and calcein, Biosens Bioelectron. 137(2019) 148-153.
[47] Z.S. Qian, L.J. Chai, Y.Y. Huang, C. Tang, J.J. Shen, J.R. Chen, H. Feng, A real-time fluorescent assay for the detection of alkaline phosphatase activity based on carbon quantum dots, Biosens Bioelectron. 68(2015) 675-680.

Caption:

1 **Scheme 1** A proposed working principle for applying NO_2-Eu-MOF NS as a selective biosensor to determine ALP activity. The fluorescence is based on the competitive coordination of Eu^{3+} between the ligands of PEPP (phosphate group) and NO_2BDC (carboxylate group) in solution and the difference UV-Vis absorption properties between PNPP and 4-NP;

2 **Fig. 1** The characterization of NO_2-Eu-MOF NS synthesized with hydrothermal method. **a-c**: the SEM images; **d-f**: the TEM images; **g-k**: the mapping images;

3 **Fig. 2** The XPS spectra of NO_2-Eu-MOF NS. **a**: the high-resolution spectra of Eu 3d; **b**: C 1s; **c**: O 1s; **d**: N 1s;

4 **Fig. 3 a:** the fluorescence spectrum of NO_2BDC, M, $Eu_x(PEPP)_y(NO_2BDC)_z$, and EuPEPP; **b**: the XRD spectra of M, $Eu_x(PEPP)_y(NO_2BDC)_z$, EuPEPP, and EuPEPP simulation. **c**: the SEM images of $Eu_x(PEPP)_y(NO_2BDC)_z$ and corresponding SEM-EDX elemental mapping result; **d**: the fluorescence spectra to show the effect of ALP activity. ALP (500 U L^{-1}, 700 U L^{-1} and 1000 U L^{-1}) was used in the hydrolysis of PNPP (10 mM) for 20 min and followed adding M. The fluorescence spectrum of M reacted with PEPP and M react with ALP was record as a control.; **e**: the UV-Vis spectra of PNPP, 4-NP and fluorescence excitation spectra of $Eu_x(PEPP)_y(NO_2BDC)_z$. M (50 μL 100 μg mL^{-1}), EuPEPP (50 μL 100 μg mL^{-1}), PEPP (10 mM), Tris-HCl buffer (50 mM, pH 9.0), excitation at 280 nm;

5 **Fig. 4** Conditions optimization of (a) PEPP concentration; (b) time for PEPP react with NO_2-Eu-MOF NS; (c) PNPP concentration; and (d) time of PNPP be hydrolyzed by ALP.

Conditions for assays: NO_2-Eu-MOF NS (50 μL, 100 μg mL^{-1}), Tris-HCl buffer (50 mM, pH 9.0), excitation at 280 nm; emission: 550-800 nm.

6 **Fig. 5** Quantitative assays of ALP activity with the as-fabricated biosensor. **a**: the fluorescence spectra with different activity of ALP; **b**: the linear relationship between ΔF and the activity of ALP. Conditions for assays: NO_2-Eu-MOF NS (50 μL, 100 μg mL^{-1}), PEPP (10 mM), PNPP (25 mM), Tris-HCl buffer (50 mM, pH 9.0), excitation at 280 nm; emission: 550-800 nm;

7 **Fig. 6** Selectivity and interferential test of proposed sensor. **a**: the selectivity test; **b**: the anti-interferential test of proposed fluorescence sensor. The concentration of Mg^{2+}, Zn^{2+}, Fe^{2+}, Cu^{2+}, S^{2-}, Thr, GSH, UA, Glu, PPi, HSA, ACP, PPase, Lys, ATP and Trp was 100 μM, 100 μM, 100 μM, 1 mM, 2.5 mM, 500 μM, 5 mM, 420 μM, 8 mM, 200 mM, 30 g L^{-1}, 10 U L^{-1},10 U L^{-1}, 500 μM, 1 μM, and 500 μM, respectively. NO_2-Eu-MOF NS (50 μL, 100 μg mL^{-1}), PEPP (10 mM), ALP (800 U L^{-1}), Tris-HCl buffer (50 mM, pH 9.0), excitation at 280 nm; emission: 550-800 nm;

8 **Table 1** A comparison of analytical methods for the determination of ALP activity

9 **Table 2** The determination of ALP activity in human serum with NO_2-Eu-MOF NS

1 **Scheme 1**

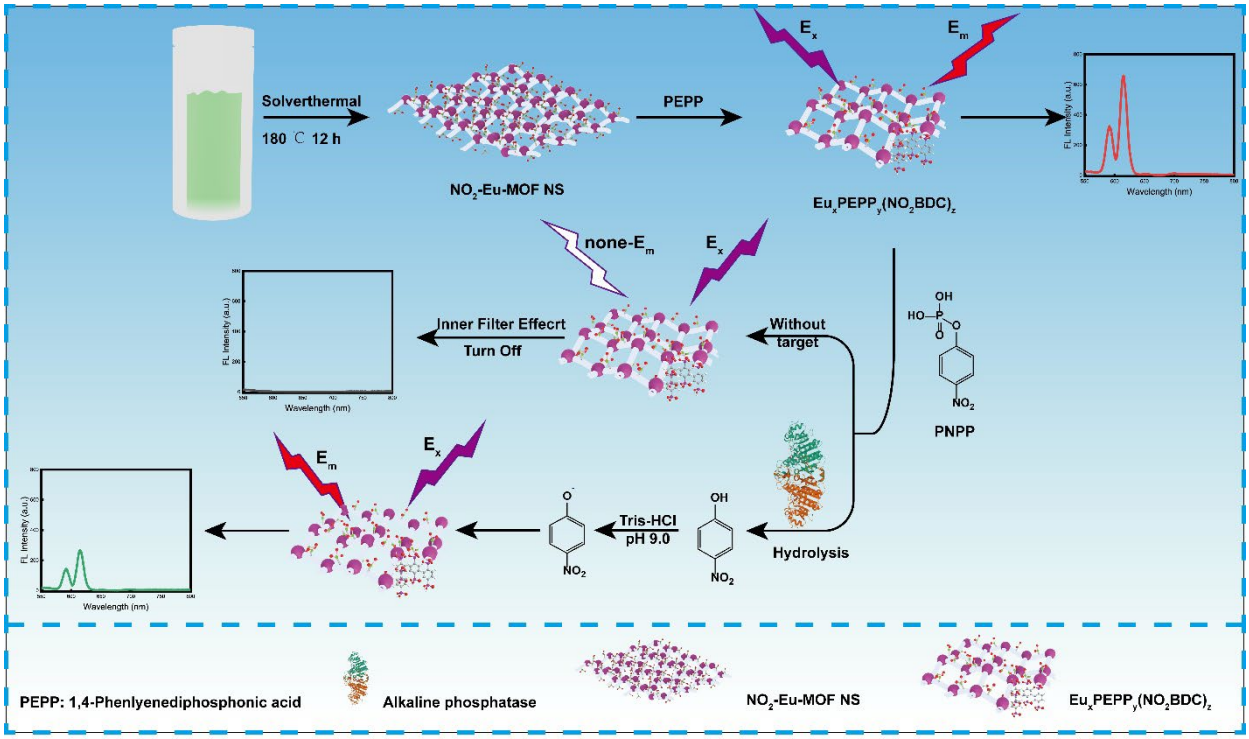
Solverthermal
180 ℃ 12 h
NO2-Eu-MOF NS
PEPP
Ex
Em
EuxPEPPy(NO2BDC)z
Wavelength (nm)
none-Em
Ex
Inner Filter Effecrt
Turn Off
Without target
PNPP
Hydrolysis
Tris-HCl
pH 9.0
Em
Ex
PEPP: 1,4-Phenlyenediphosphonic acid
Alkaline phosphatase
NO2-Eu-MOF NS
EuxPEPPy(NO2BDC)z

2 **Fig. 1**

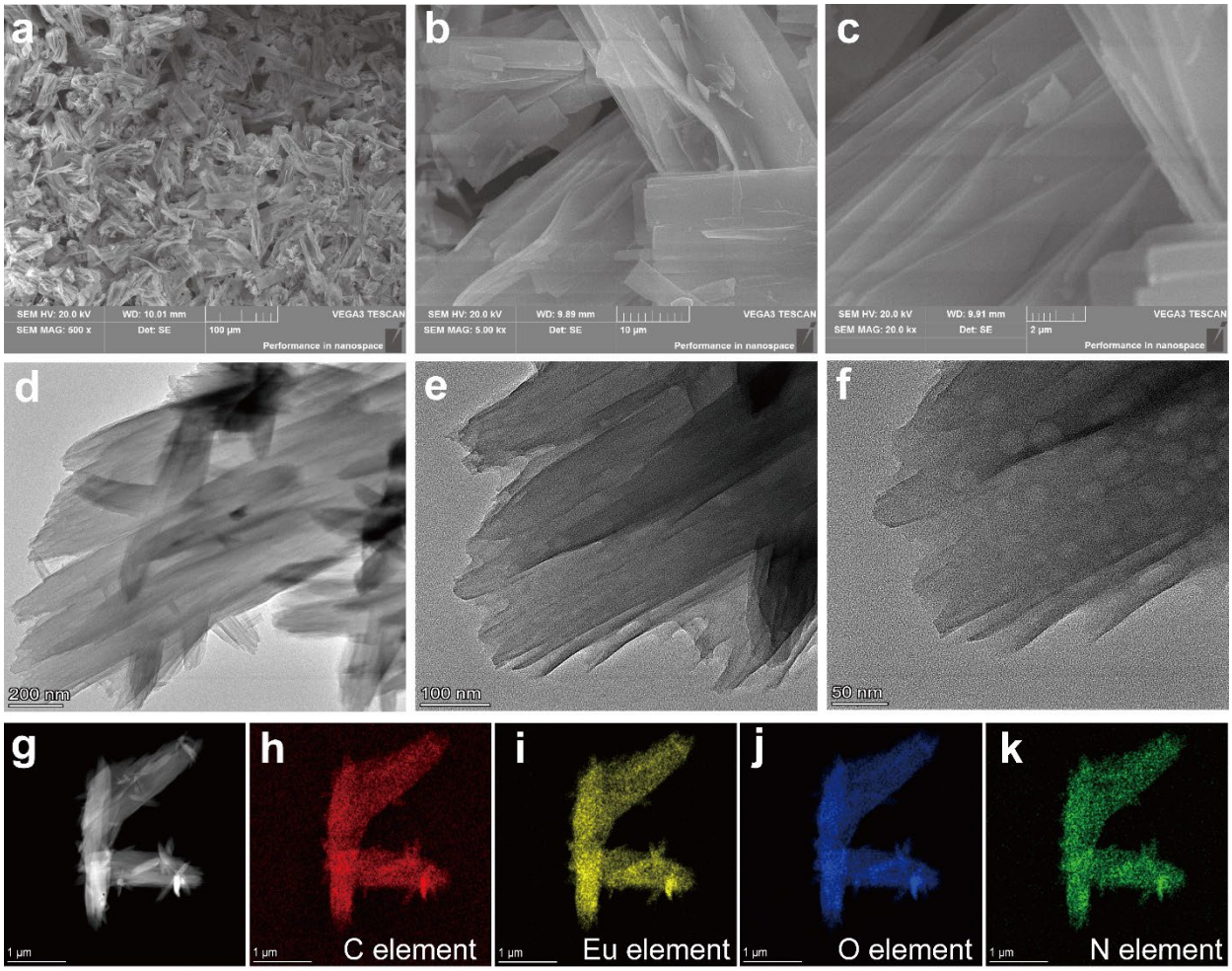
a
SEM HV: 20.0 kV
WD: 10.01 mm
VEGA3 TESCAN
SEM MAG: 500 x
Det: SE
100 µm
Performance in nanospace
b
SEM HV: 20.0 kV
WD: 9.89 mm
VEGA3 TESCAN
SEM MAG: 5.00 kx
Det: SE
10 µm
Performance in nanospace
c
SEM HV: 20.0 kV
WD: 9.91 mm
VEGA3 TESCAN
SEM MAG: 20.0 kx
Det: SE
2 µm
Performance in nanospace
d
200 nm
e
100 nm
f
50 nm
g
1 µm
h
1 µm
C element
i
1 µm
Eu element
j
1 µm
O element
k
1 µm
N element

3 **Fig. 2**

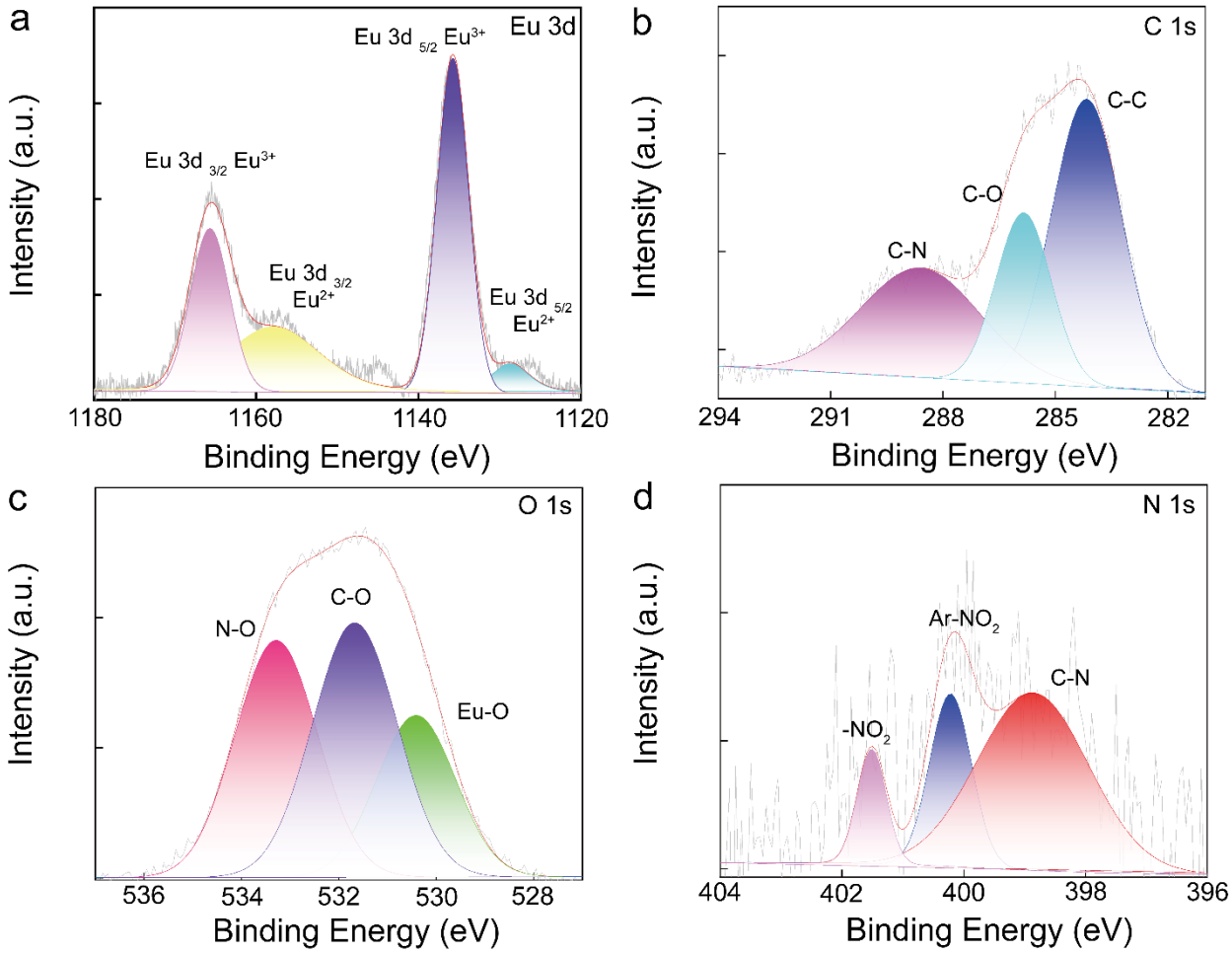
a
Eu 3d
Eu 3d 5/2 Eu3+
Eu 3d 3/2 Eu3+
Eu 3d 3/2 Eu2+
Eu 3d 5/2 Eu2+
Intensity (a.u.)
1180
1160
1140
1120
Binding Energy (eV)
b
C 1s
C-C
C-O
C-N
Intensity (a.u.)
294
291
288
285
282
Binding Energy (eV)
c
O 1s
N-O
C-O
Eu-O
Intensity (a.u.)
536
534
532
530
528
Binding Energy (eV)
d
N 1s
Ar-NO2
C-N
-NO2
Intensity (a.u.)
404
402
400
398
396
Binding Energy (eV)

4 **Fig. 3**

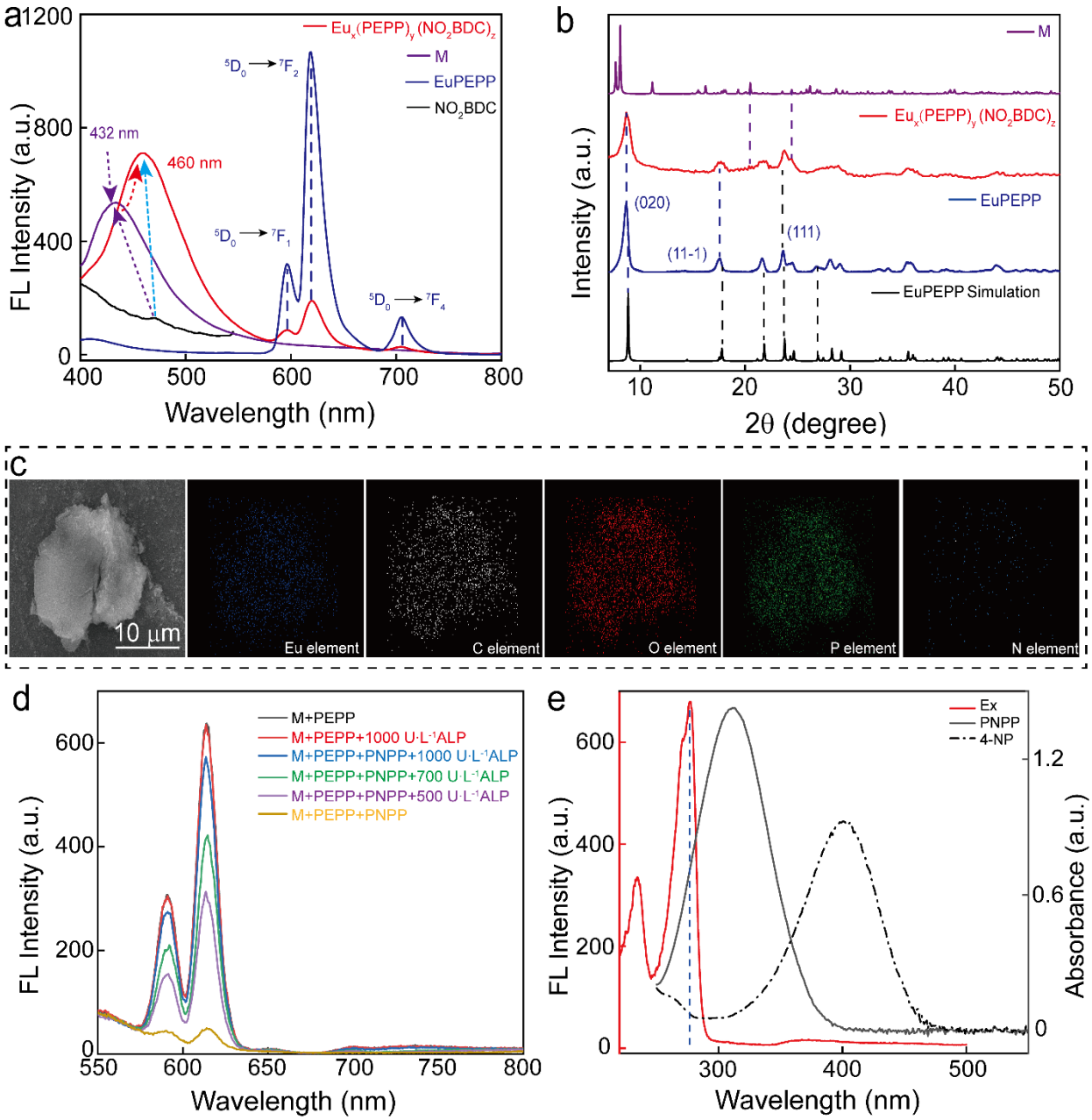
a
Eu$_x$(PEPP)$_y$(NO$_2$BDC)$_z$
M
EuPEPP
NO$_2$BDC
$^5D_0 \rightarrow {}^7F_2$
$^5D_0 \rightarrow {}^7F_1$
$^5D_0 \rightarrow {}^7F_4$
432 nm
460 nm
FL Intensity (a.u.)
Wavelength (nm)
b
M
Eu$_x$(PEPP)$_y$(NO$_2$BDC)$_z$
EuPEPP
EuPEPP Simulation
(020)
(11-1)
(111)
Intensity (a.u.)
2θ (degree)
c
10 μm
Eu element
C element
O element
P element
N element
d
M+PEPP
M+PEPP+1000 U·L^{-1}ALP
M+PEPP+PNPP+1000 U·L^{-1}ALP
M+PEPP+PNPP+700 U·L^{-1}ALP
M+PEPP+PNPP+500 U·L^{-1}ALP
M+PEPP+PNPP
FL Intensity (a.u.)
Wavelength (nm)
e
Ex
PNPP
4-NP
FL Intensity (a.u.)
Absorbance (a.u.)
Wavelength (nm)

5 **Fig. 4**

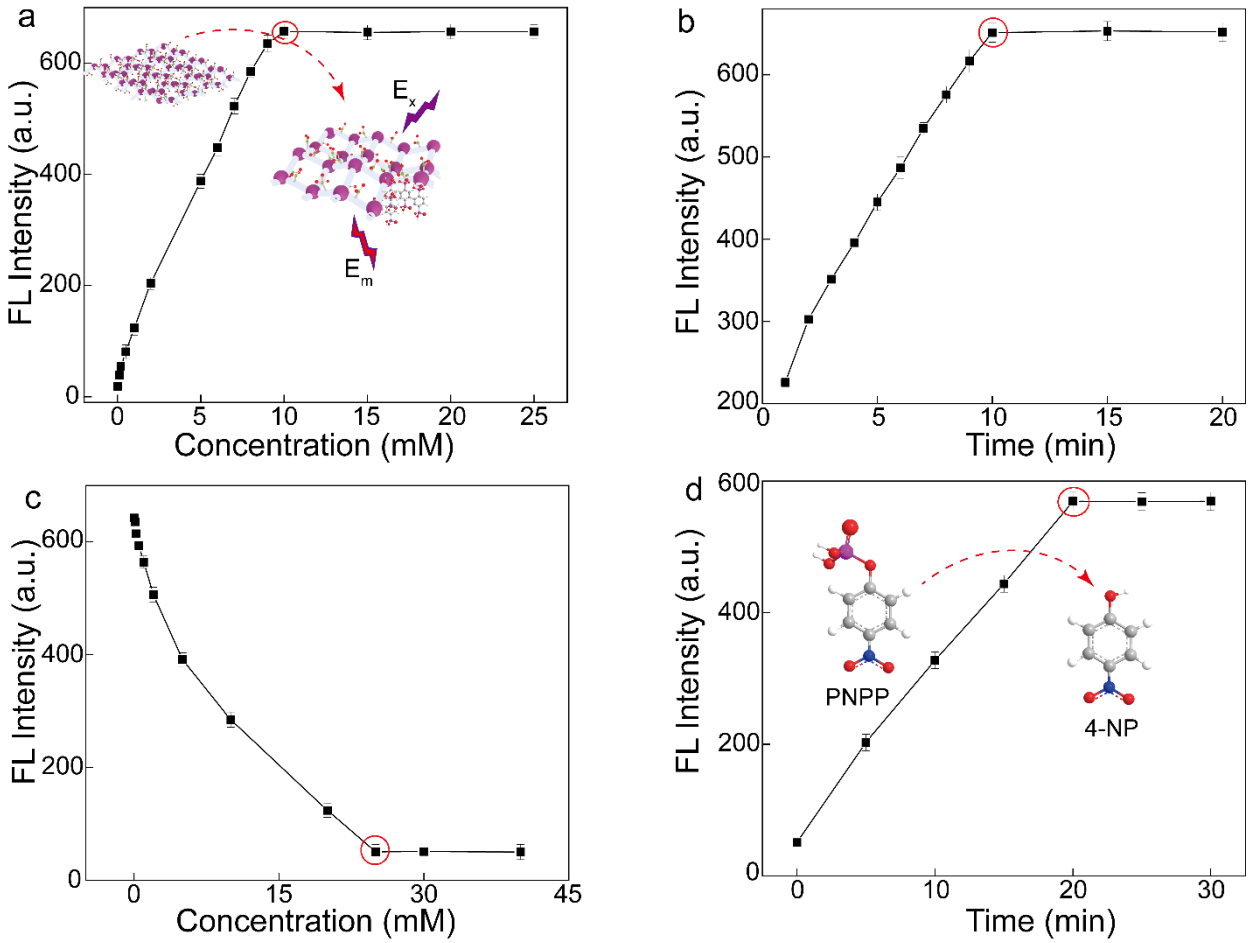
a
FL Intensity (a.u.)
Concentration (mM)
E_x
E_m
b
FL Intensity (a.u.)
Time (min)
c
FL Intensity (a.u.)
Concentration (mM)
d
FL Intensity (a.u.)
Time (min)
PNPP
4-NP

6 **Fig. 5**

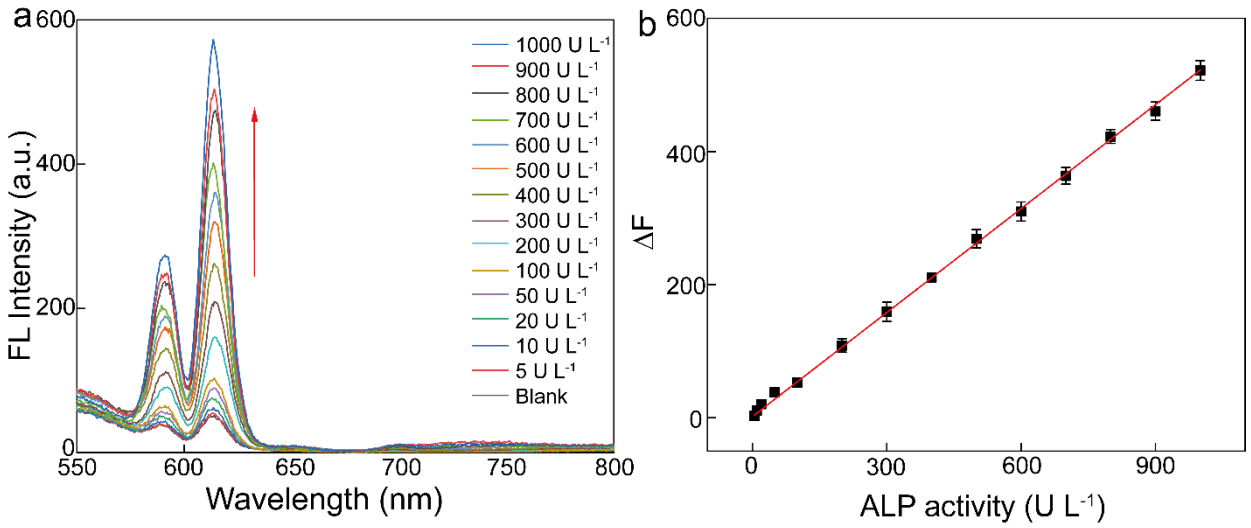
a
FL Intensity (a.u.)
Wavelength (nm)
1000 U L-1
900 U L-1
800 U L-1
700 U L-1
600 U L-1
500 U L-1
400 U L-1
300 U L-1
200 U L-1
100 U L-1
50 U L-1
20 U L-1
10 U L-1
5 U L-1
Blank
b
ΔF
ALP activity (U L-1)

7 **Fig. 6**

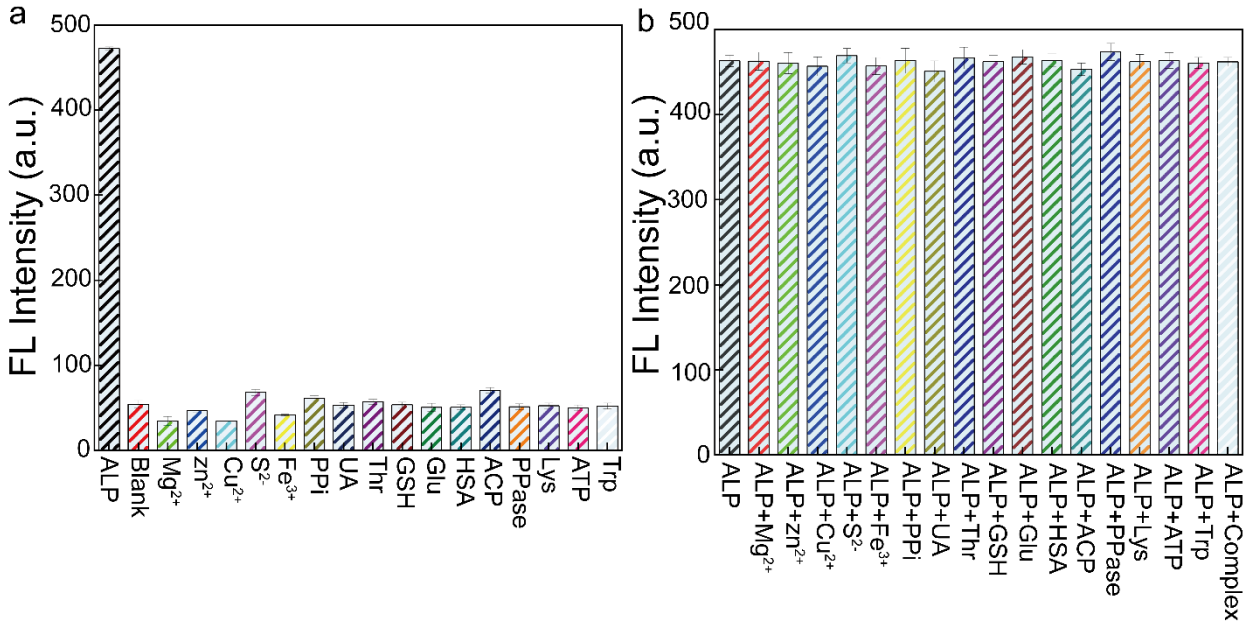
a
FL Intensity (a.u.)
0
100
200
300
400
500
ALP
Blank
Mg2+
Zn2+
Cu2+
S2-
Fe3+
PPi
UA
Thr
GSH
Glu
HSA
ACP
PPase
Lys
ATP
Trp
b
FL Intensity (a.u.)
0
100
200
300
400
500
ALP
ALP+Mg2+
ALP+Zn2+
ALP+Cu2+
ALP+S2-
ALP+Fe3+
ALP+PPi
ALP+UA
ALP+Thr
ALP+GSH
ALP+Glu
ALP+HSA
ALP+ACP
ALP+PPase
ALP+Lys
ALP+ATP
ALP+Trp
ALP+Complex

8 **Table 1**

Method	Material	Dynamic Range ($U\ L^{-1}$)	LOD ($U\ L^{-1}$)	Reference
ECL	-	0.002-50	0.0007	[1]
ECL	-	20-1500	3	[5]
Colorimetric	PDA	10-100	5.4	[42]
Colorimetric	Au/Ag nanorod	20-500	3.3	[43]
Colorimetric	$Cu(BCDS)_2^{2-}$	0-220	1.27	[44]
Colorimetric	Cu(II)-phenanthroline	0-200	3.5	[45]
Fluorescence	Ag_2S QDs	2-100	1.28	[46]
Fluorescence	Carbon QDs	16.7–782.6	1.1	[47]
Fluorescence	NO_2-Eu-MOF NS	5-1000	1.1	This Work

9 **Table 2**

Sample	Detected ($U\ L^{-1}$)	Reference ($U\ L^{-1}$)	Spiked ($U\ L^{-1}$)	Total found ($U\ L^{-1}$)	Recovery	RSD
1	88.20	90	10.0	99.50	95.0%	4.9%
			50.0	138.10	96.2%	4.5%
			100.0	191.00	101.0%	5.2%
2	76.10	78	10.0	87.50	95.0%	4.6%
			50.0	129.80	103.6%	5.3%
			100.0	180.60	102.6%	5.0%
3	59.30	60	10.0	69.90	99.0%	5.4%
			50.0	110.80	101.6%	4.8%
			100.0	162.50	102.5%	5.5%